Dynamics of the two-mass model of the vocal folds: Equilibria, bifurcations, and oscillation region

Jorge C. Lucero
QI 27 conj. 12 casa 13, Lago Sul, Brasilia DF, CEP 71675-120, Brazil

(Received 28 September 1992; accepted for publication 26 July 1993)

The dynamics of the large-amplitude oscillation of the vocal folds is analyzed using the two-mass model. First, the equilibrium positions are determined in the case of a rectangular prephonatory glottis, and the existence of two equilibrium positions besides the rest position is shown. Their stability is examined and a bifurcation diagram is derived with a normalized subglottal pressure and a coupling coefficient as control parameters. Phase plane plots are shown to illustrate the results. The cases of convergent and divergent prephonatory glottis are then briefly considered. The main results are finally discussed relative to previous analytical works; it is shown that they disprove the previous oscillation theory based on the existence of a glottal negative differential resistance.

PACS numbers: 43.70.Aj, 43.70.Bk

INTRODUCTION

The two-mass model of the vocal folds (Ishizaka and Matsudaira, 1972; Ishizaka and Flanagan, 1972) has been used in the past years to study the vocal fold oscillation in the production of voice. The capability of this well-known model to reproduce the oscillation in detail has been successfully demonstrated, and it has been widely used as a glottal source for speech synthesis (Ishizaka and Flanagan, 1972, 1977; Ishizaka and Isshiki, 1976; Koizumi *et al.*, 1987; Miller *et al.*, 1988).

A number of analytical treatments of this model have been presented, intending to explain its basic dynamics and to build a theory of the vocal fold oscillation (Ishizaka and Matsudaira, 1972; Ishizaka, 1981; Ishizaka *et al.*, 1987). However, because of the complexity of the equations, the analyses have been restricted to small-amplitude oscillations around the rest position of the vocal folds. In this approach, the equations of motion are first linearized at the rest position, whose instability is then studied through the Routh–Hurwitz criterion or similar techniques. The conditions of instability thus obtained have been considered as the parameters for the generation of the oscillation, or threshold conditions.

According to these analyses, the oscillation dynamics could be described through a Hopf bifurcation: A stable equilibrium position (the rest position) becomes unstable at a certain value of a parameter such as the subglottal pressure, and at the same time a stable limit cycle is generated (Guckenheimer and Holmes, 1983). It has been shown that at a threshold value of the subglottal pressure, two complex conjugate roots of the corresponding characteristic equation cross the imaginary axis with their real parts becoming positive (Ishizaka *et al.*, 1987), which indicates the existence of this bifurcation.

However, using a related plank model and considering the general case of large-amplitude oscillations, the existence of a second equilibrium position and additional bifurcation phenomena have been found (Lucero and Gotoh, 1992; Lucero, 1993). Those results imply a more complex oscillation dynamics than the single Hopf bifurcation described above.

In this paper, a large-amplitude analysis of the dynamics of the two-mass model is presented to provide a more complete description of its equilibria and bifurcations. This study intends to serve as a mathematical basis for future studies on the vocal fold oscillation. It is important to note here that the suitability of the two-mass model to study the vocal fold oscillation has been questioned previously; e.g., Titze (1988) has pointed out the difficulty in correlating the model parameters to the vocal fold anatomy. However, it is a relatively simple model that permits us to study the oscillation analytically even without the small-amplitude restriction, and including the glottal closure. Keeping its limitations in mind, it is adopted for a first analysis of the oscillation dynamics. The results of this analysis will be discussed and examined relative to previous analytical works.

I. EQUATIONS OF MOTION

Figure 1 shows a simplified diagram of the two-mass model. The equations developed by Ishizaka and Flanagan (1972) for this model are adopted with their notation. However, the following assumptions are made to simplify the analysis.

(i) The inertia of the glottal air is small and the glottal flow is considered quasisteady (Flanagan, 1972).

(ii) The supraglottal pressure is zero (atmospheric). This assumption neglects the vocal tract load and corresponds to the case of an excised larynx. This is justified considering that the vocal fold oscillation also occurs in excised larynges, as observed by Baer (1981).

(iii) The cubic nonlinearity of the elastic restoring forces of the tissues is small (the nonlinearity introduced by the collision between the opposite vocal folds is maintained).

 0001-4966/93/94(6)/3104/8/$6.00

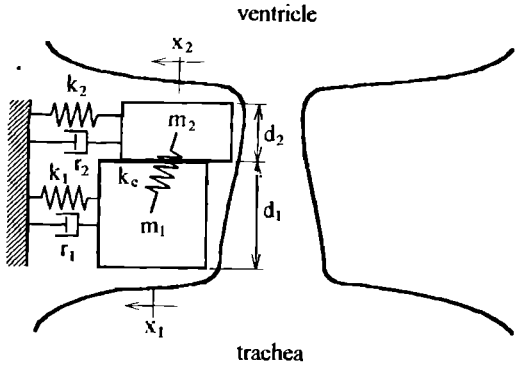

FIG. 1. Diagram of the two-mass model of the vocal folds. m_1 and m_2: lower and upper masses of the vocal fold. r_1 and r_2: viscous damping coefficients. k_1, k_2, and k_c: stiffness coefficients. d_1 and d_2: thickness of masses m_1 and m_2. x_1 and x_2: displacement of masses m_1 and m_2 from their rest position (Ishizaka and Flanagan, 1972).

(iv) The pressure recovery at the glottal outlet is small (Titze, 1988).

(v) The glottal viscous resistances are small. This assumption has been made in previous analyses (e.g., Ishizaka and Matsudaira, 1972; Titze, 1988), where only small-amplitude oscillations around a wide open glottis are considered. In that case, the viscous losses are small and can be neglected; however, the present analysis does not have that amplitude restriction, and a different justification is required. This will be done through the numerical solution of the equations of motion, showing that the inclusion of the viscous resistances does not alter significantly the analytical results.

With the above assumptions, the equations of motion become

$$m_1\left(\frac{d^2x_1}{dt^2}\right)+r_1\left(\frac{dx_1}{dt}\right)+s_1+k_c(x_1-x_2)=F_1, \tag{1a}$$

$$m_2\left(\frac{d^2x_2}{dt^2}\right)+r_2\left(\frac{dx_2}{dt}\right)+s_2+k_c(x_2-x_1)=F_2, \tag{1b}$$

where x_i $(i=1,2)$ is the displacement of mass m_i from its rest position, r_i is its viscous damping coefficient, k_c is the coupling stiffness between both masses, F_i is the driving force acting on m_i, s_i is the elastic restoring force given by

$$s_i=\begin{cases} k_i x_i, & \text{for } x_i > -x_{i0} \\ k_i x_i + h_i(x_i+x_{i0}), & \text{for } x_i \leqslant -x_{i0} \end{cases} \quad (i=1,2), \tag{2}$$

k_i is the stiffness in the open glottis condition, h_i is the stiffness introduced by the collision between the vocal folds, and x_{i0} is the half-width of the glottis at mass m_i at its rest or prephonatory position. The driving force F_i is given by

$$F_1=\begin{cases} l_g d_1 P_s f_p, & \text{for } x_1 > -x_{10} \text{ and } x_2 > -x_{20}, \\ l_g d_1 P_s, & \text{otherwise,} \end{cases} \tag{3a}$$

$$F_2=\begin{cases} l_g d_2 P_s, & \text{for } x_1 > -x_{10} \text{ and } x_2 \leqslant -x_{20}, \\ 0, & \text{otherwise,} \end{cases} \tag{3b}$$

where d_i is the thickness of mass m_i, l_g is the length of the masses, P_s is the subglottal pressure, and f_p is the function

$$f_p=\frac{(x_1+x_{10})^2-(x_2+x_{20})^2}{(x_1+x_{10})^2+\kappa(x_2+x_{20})^2}, \tag{4}$$

where $\kappa=0.37$ (Ishizaka and Flanagan, 1972) is a pressure loss factor for the area contraction at the glottal inlet.

II. EQUILIBRIUM POSITIONS

A. Open glottis

The open glottis condition is considered here, i.e., $x_1 > -x_{10}$ and $x_2 > -x_{20}$. The equilibrium positions are obtained by setting the derivatives to zero in the equations of motion (1a) and (1b), and using the expressions of the elastic restoring forces and driving forces in Eqs. (2) and (3a), (3b), respectively, for the open glottis. Hence,

$$k_1 x_{1e}+k_c(x_{1e}-x_{2e})=l_g d_1 P_s \frac{(x_{1e}+x_{10})^2-(x_{2e}+x_{20})^2}{(x_{1e}+x_{10})^2+\kappa(x_{2e}+x_{20})^2}, \tag{5a}$$

$$k_2 x_{2e}+k_c(x_{2e}-x_{1e})=0, \tag{5b}$$

where x_{ie} $(i=1,2)$ denotes the equilibrium positions.

From Eq. (5b) we obtain the relation

$$x_{2e}=\alpha x_{1e}, \tag{6}$$

where α is the coupling coefficient

$$\alpha=k_c/(k_2+k_c). \tag{7}$$

Using Eq. (6), x_{2e} can be eliminated from Eq. (5a), which is then rewritten

$$(y_{1e}-1)=H\frac{\beta^2 y_{1e}^2-y_{2e}^2}{\beta^2 y_{1e}^2+\kappa y_{2e}^2}, \tag{8}$$

where the displacement variable has been changed to

$$y_i=1+x_i/x_{i0} \quad (i=1,2) \tag{9}$$

[the additional subindex e in Eq. (8) denotes the equilibrium positions], and the other parameters are given by

$$\beta=x_{10}/x_{20}, \tag{10}$$

$$H=p_s/(1+\alpha k_2/k_1), \tag{11}$$

$$p_s=l_g d_1 P_s/k_1 x_{10}. \tag{12}$$

The variable y_i may be considered as a normalized displacement coordinate, and the parameter p_s as a normalized subglottal pressure. The relation between y_{1e} and y_{2e} is given by

$$y_{2e}=\alpha\beta(y_{1e}-1)+1. \tag{13}$$

In the following analysis, the simple case of a rectangular prephonatory glottis, i.e., $\beta=1$ $(x_{10}=x_{20})$, will be considered. In this particular case, the above equations take a simple form permitting the analytical treatment. The cases of convergent and divergent prephonatory glottis will be briefly examined in a later section,.

Letting $\beta=1$ in Eqs. (8) and (13) and solving them for y_{1e} and y_{2e}, we obtain a first solution

$$y_{1e}=y_{2e}=1, \tag{14}$$

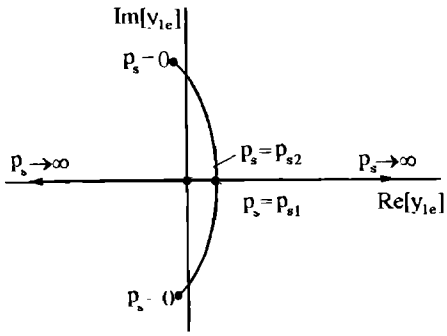

FIG. 2. Diagram of the roots of Eq. (15), with the normalized subglottal pressure p_s as a parameter. At $p_s=p_{s1}$ one of the roots is zero; at $p_s=p_{s2}$ both roots coincide.

which corresponds to the rest position $x_{1e}=x_{2e}=0$. For clarity in the following explanations, this will be called equilibrium position R. The other solutions are given by the quadratic equation for y_{1e}:

$$(1+\kappa\alpha^2)y_{1e}^2+(1-\alpha)[2\kappa\alpha-(1+\alpha)H]y_{1e} -(1-\alpha)^2(H-\kappa)=0, \quad (15)$$

together with Eq. (13).

Let us examine the solutions of Eq. (15), schematically plotted in Fig. 2. For a value of p_s (or H) large enough, the coefficients of the second and third terms are negative, which indicates the existence of two real solutions with opposite signs. However, from Eq. (9) we have that a negative value of y_{1e} implies $x_{1e}<-x_{10}$, which corresponds to a closed glottis. Since the above equations correspond to the open glottis, this solution is invalid. The second positive solution implies $x_{1e}>-x_{10}$ and, since by applying Eq. (6) we also have $x_{2e}>-x_{20}$ (recall the assumption $x_{10}=x_{20}$), this is a valid solution. This solution implies the existence of a second equilibrium position, which will be called equilibrium position A. When this second equilibrium position becomes coincident with the rest position at $y_{1e}=y_{2e}=1$ a bifurcation occurs, as will be shown later. Letting $y_{1e}=1$ in Eq. (15) we obtain

$$H=(1+\kappa)/2(1-\alpha). \quad (16)$$

If we decrease the value of p_s (or H), both solutions of Eq. (15) come closer together. When the third term becomes zero at $H=\kappa$, the previous negative real solution crosses the imaginary axis. The value of p_s at this point will be denoted as p_{s2}. Then, for $p_s<p_{s2}$, we have three equilibrium positions; the third equilibrium position will be called equilibrium position B. Decreasing p_s further, both solutions become coincident when the discriminant of Eq. (15) is zero, and then complex, in which case only one equilibrium position exists: equilibrium position R at the rest position. The value of p_s at the point of coincidence of both solutions will be called p_{s1}. Then, the regions of existence of equilibrium positions A and B are $p_s\geqslant p_{s1}$ and $p_{s1}\leqslant p_s<p_{s2}$, respectively.

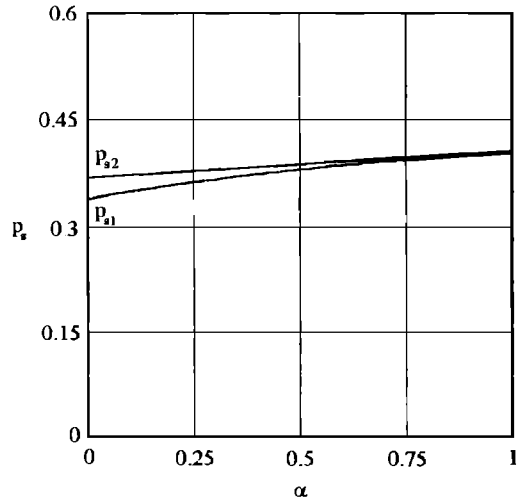

FIG. 3. Values p_{s1} and p_{s2} of the normalized subglottal pressure versus the coupling ratio α, for $k_1/k_2=10$ and $\beta=1$ (rectangular prephonatory glottis). Equilibrium position A exists for $p_s\geqslant p_{s1}$, and equilibrium position B for $p_{s1}\leqslant p_s<p_{s2}$.

B. Closed glottis

The closed glottis is considered next, i.e., $x_1\leqslant -x_{10}$ or $x_2\leqslant -x_{20}$. We proceed similarly as before, setting the derivatives in the equations of motion (1a) and (1b) equal to zero, and introducing the expressions of the elastic restoring forces and driving forces in Eqs. (2) and (3a), (3b), respectively, for this condition. The resultant equations are linear in this case and easy to solve. However, the solutions obtained are such that $x_{1e}>-x_{10}$ and $x_{2e}>-x_{20}$, and therefore do not correspond to the closed glottis. We can then conclude that the equilibrium positions found in the open glottis are the only ones present in the model.

C. Numerical examples

Numerical examples of the previous results are shown in Figs. 3 and 4.

In Fig. 3, the values of p_{s1} and p_{s2} are plotted as a function of α. A ratio $k_1/k_2=10$ was used in the calculations, given by Ishizaka and Flanagan (1972) as a typical value for the two mass model. Typical values for the other parameters are listed in Table I. The values of p_{s1} and p_{s2} divide the graph in three regions. Below p_{s1} only one equilibrium position exists, equilibrium position R at the rest position. In the small region between p_{s1} and p_{s2} we have three equilibrium positions, R, A, and B; and above p_{s2} we have two equilibrium positions, R and A. Using the values of Table I, the typical condition of the model is expressed by $\alpha=0.76$ and $p_s=1.91$. These values correspond to a point above p_{s2}; hence, two equilibrium positions, R and A, exist in the typical condition.

In Fig. 4, the location of the equilibrium positions in the y_1-y_2 plane is shown, for $k_1/k_2=10$, $\alpha=0.76$, and p_s as a parameter. Equilibrium position B is located close to the y_2 axis and cannot be shown with clarity in this graph. At a value of $p_s=0.40$, equilibrium positions A and B cancel

TABLE I. Typical values of the parameters of the two-mass model (Ishizaka and Flanagan, 1972).

Parameter	Value
Length l_g	1.4 cm
Width	
d_1	0.25 cm
d_2	0.05 cm
Half glottal width at rest (prephonatory position)	
x_{10}	0.02 cm
x_{20}	0.02 cm
Subglottal pressure P_s	7840 dyn/cm^2
Mass	
m_1	0.125 g
m_2	0.025 g
Stiffness	
k_1	80 kdyn/cm
k_2	8 kdyn/cm
k_c	25 kdyn/cm
Damping ratio	
$\zeta_1=r_1/[2(m_1k_1)^{1/2}]$	0.1
$\zeta_2=r_2/[2(m_2k_2)^{1/2}]$	0.6
Pressure loss factor κ	0.37

each other. Note also that equilibrium positions R and A coincide at $p_s=3.07$.

III. STABILITY AND BIFURCATIONS

A. Characteristic equation

The stability of the equilibrium positions can be analyzed considering only the linear part of the equations of motion in the neighborhood of those positions (Guckenheimer and Holmes, 1983). Since all the equilibrium positions are located in the open glottis, only the equations of motion for this condition need to be considered, given by Eqs. (1a)–(4) with $x_i > -x_{i0}$ $(i=1,2)$. In these equations there is a nonlinear factor, the function f_p given by Eq. (4). This function is then linearized, first, by the usual technique of letting

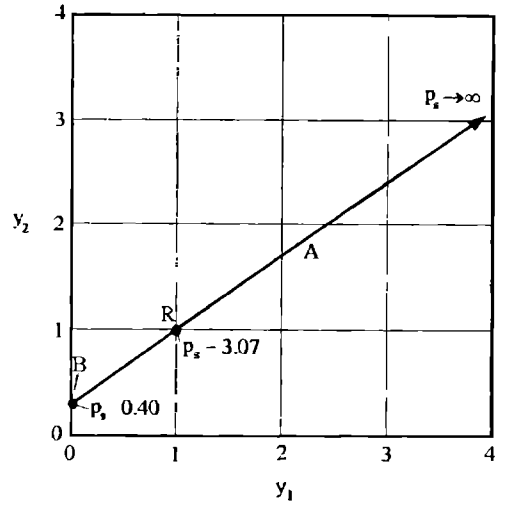

FIG. 4. Location of the equilibrium positions R, A, and B in the y_1-y_2 plane with the normalized subglottal pressure p_s as a parameter, for $k_1/k_2=10$, $\alpha=0.76$, and $\beta=1$ (rectangular prephonatory glottis).

$$x_i=x_{ie}+\varepsilon_i \quad (i=1,2), \tag{17}$$

where ε_i denotes a small displacement from the equilibrium position x_{ie}, and, next, by taking the linear term of its Taylor expansion at x_{ie}. Replacing the result in the equations of motion, we obtain the linear equations

$$m_1\left(\frac{d^2\varepsilon_1}{dt^2}\right)+r_1\left(\frac{d\varepsilon_1}{dt}\right)+k_1\varepsilon_1+k_c(\varepsilon_1-\varepsilon_2)$$
$$=p_sk_1(D_1\varepsilon_1+D_2\varepsilon_2), \tag{18a}$$

$$m_2\left(\frac{d^2\varepsilon_2}{dt^2}\right)+r_2\left(\frac{d\varepsilon_2}{dt}\right)+k_2\varepsilon_2+k_c(\varepsilon_2-\varepsilon_1)=0, \tag{18b}$$

where, from Eq. (4) and using also Eq. (9),

$$D_1=x_{10}\frac{\delta f_p}{\delta x_1}(x_{1e},x_{2e})=\frac{2(1+\kappa)\beta^2y_{1e}y_{2e}^2}{(\beta^2y_{1e}^2+\kappa y_{2e}^2)^2}, \tag{19a}$$

$$D_2=x_{10}\frac{\delta f_p}{\delta x_2}(x_{1e},x_{2e})=-\frac{2(1+\kappa)\beta^3y_{1e}^2y_{2e}}{(\beta^2y_{1e}^2+\kappa y_{2e}^2)^2}. \tag{19b}$$

The characteristic equation corresponding to Eqs. (18a) and (18b) is

$$s^4+\left(\frac{r_1}{m_1}+\frac{r_2}{m_2}\right)s^3+\left(\frac{k_1+k_c-p_sk_1D_1}{m_1}+\frac{k_2+k_c}{m_2}+\frac{r_1r_2}{m_1m_2}\right)s^2$$
$$+\left(\frac{r_1}{m_1}\frac{k_2+k_c}{m_2}+\frac{r_2}{m_2}\frac{k_1+k_c-p_sk_1D_1}{m_1}\right)s$$
$$+\frac{k_1+k_c-p_sk_1D_1}{m_1}\frac{k_2+k_c}{m_2}-\frac{k_c}{m_1}\frac{k_c+p_sk_1D_2}{m_2}=0. \tag{20}$$

The stability of each equilibrium position can then be determined by examining the roots of the above characteristic equation.

B. Analysis of stability and bifurcations

The analysis is done considering the typical condition given by the values of Table I and adopting the normalized subglottal pressure p_s and the coupling parameter α as the control parameters. Main results are illustrated by the bifurcation diagram of Fig. 5, explained in the following paragraphs.

The broken curves for p_{s1} and p_{s2} were obtained previously in Fig. 3; we saw that equilibrium position A exists above curve p_{s1}, and equilibrium position B in the small region between curves p_{s1} and p_{s2}. Curve p_{s1} indicates a bifurcation of the saddle-node type, where the two equilibrium positions A and B coincide and cancel each other (Guckenheimer and Holmes, 1983).

Curve EF indicates the points at which two complex conjugate roots of the characteristic equation for equilibrium position R cross the imaginary axis and their real parts become positive. Below this curve, R is stable. At this curve it becomes unstable, and at the same time a stable limit cycle appears (shown in the next section through numerical computations); i.e., curve EF indicates a Hopf bifurcation. This bifurcation has already been found analytically in previous works (e.g., Ishizaka *et al.*, 1987), as

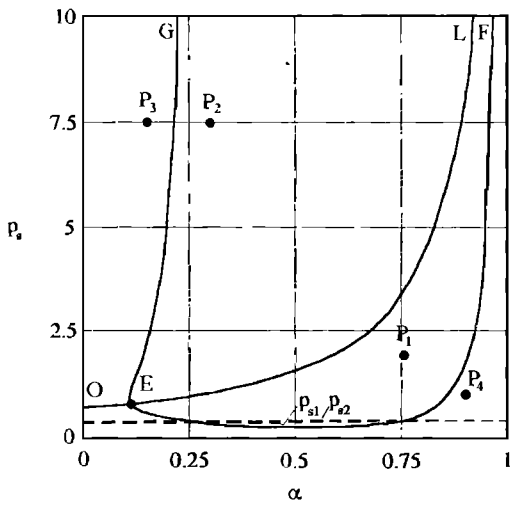

FIG. 5. Bifurcation diagram with the normalized subglottal pressure p_s and coupling ratio α as control parameters, for the typical values of Table I. Curve EF: Hopf bifurcation for equilibrium position R. Curve EG: Hopf bifurcation for equilibrium position A. Curve OL: transcritical bifurcation for equilibrium positions R and A. Curve p_{s1}: minimum value of p_s for the existence of equilibrium positions A and B (saddle-node bifurcation). Curve p_{s2}: maximum value of p_s for the existence of equilibrium position *B*.

discussed in the Introduction. It shows the existence of an oscillation threshold pressure, or minimum value of the subglottal pressure required to generate the oscillation.

Curve EG also indicates a Hopf bifurcation, but in this case equilibrium position A is involved. In the left side of this curve, this position is stable; at this curve it bifurcates into an unstable position and a stable limit cycle (the same limit cycle of bifurcation EF).

Curve OL indicates the points at which equilibrium positions R and A coincide, expressed by Eq. (16). In this case we have $y_{1e}=y_{2e}=1$, and replacing in Eqs. (19a) and (19b) we obtain $D_1=-D_2=2/(1+\kappa)$. Replacing this equation in the last term of the characteristic equation (20) and also using Eq. (16), it can be shown that the last term vanishes, which implies that one of the roots is zero. In other words, when equilibrium positions R and A coincide, a real root of their characteristic equation changes its sign. In the case of equilibrium position R the root is negative in the lower side of OL and positive in the upper side, whereas in the case of equilibrium position A the signs are opposite. Considering only the portion OE, we have that position R is stable in the lower side and unstable in the upper side, whereas position A has opposite properties. This shows the existence of a transcritical bifurcation at OE: two equilibrium positions coincide and exchange their stability properties (Guckenheimer and Holmes, 1983). In the portion EL there is an exchange in the number of roots with positive real parts for each equilibrium position; however, both equilibrium positions are already unstable on both sides of the line, and hence this bifurcation has no visible effect. The transcritical bifurcation at OL can be interpreted in a broader sense as responsible for the exchange in the equilibrium positions involved in the Hopf bifurcations at EF and EG.

According to this bifurcation diagram, the oscillation region is then the region of existence of the limit cycle, delimited by the Hopf bifurcations EF (lower and right limit) and EG (left limit). It can be clearly seen that it is more restricted than the instability region of equilibrium position R, in the upper side of OEF. We have then the important result that the instability of the equilibrium position R alone is not enough to generate the oscillation. This result points out the limitations of previous analyses with the assumption of small amplitude oscillations around the rest position, and justifies the present large amplitude approach.

The values of α and p_s for point E can be used as indicators of the limits of the oscillation region. These values can be calculated from the characteristic equation (20) setting to zero the last two terms (at point E the two roots related to each of the Hopf bifurcations are equal to zero), with the result

$$\alpha=\frac{1+r_1/r_2}{2+k_1/k_2}, \tag{21}$$

$$p_s=\frac{1+\kappa}{2}\left(\frac{(k_1/k_2)(2+k_1/k_2)+1+r_1/r_2}{(k_1/k_2)(2+k_1/k_2-1-r_1/r_2)}\right). \tag{22}$$

Using the typical values we obtain $\alpha=0.18$ and $p_s=0.86$, which correspond to the case of Fig. 5.

C. Phase plane plots

Examples of the oscillation in the y_1-y_2 plane for different values of the parameters α and p_s are plotted in Figs. 6–9 to illustrate the above results. The plots were obtained solving the equations of motion of the two-mass model through numerical methods, including the glottal viscous resistances neglected in the analysis. Since the results of the numerical computations are, in general, in good agreement with the analytical results, we can conclude that the neglect of the viscous resistances does not introduce a significant alteration. The analytical locations of equilibrium positions R and A are indicated in the plots (equilibrium position R is always at $y_{1e}=y_{2e}=1$).

The plot in Fig. 6 was obtained using the typical values $\alpha=0.76$ and $p_s=1.91$ (point P_1 in Fig. 5). The analytical location of equilibrium position A is $y_{1e}=0.55$ and $y_{2e}=0.66$.

In Fig. 7, the values $\alpha=0.3$ and $p_s=7.5$ (point P_2 in Fig. 5) were used, which corresponds to a point near the Hopf bifurcation for equilibrium position A. This is also suggested by the plot, where we can see that equilibrium position R is outside the limit cycle, whereas equilibrium position A, at $y_{1e}=6.75$ and $y_{2e}=2.72$, is located near its center.

In Fig. 8, the values $\alpha=0.15$ and $p_s=7.5$ (point P_3 in Fig. 5) were used, which correspond to the region where equilibrium position R is unstable and equilibrium position A is stable, as confirmed by the plot. The real location of equilibrium position A is at the center of the spiral trajectory, with the coordinates $y_{1e}=7.28$ and $y_{2e}=1.64$. This result is close to the analytical result $y_{1e}=7.72$ and $y_{2e}=2.01$ indicated by point A.

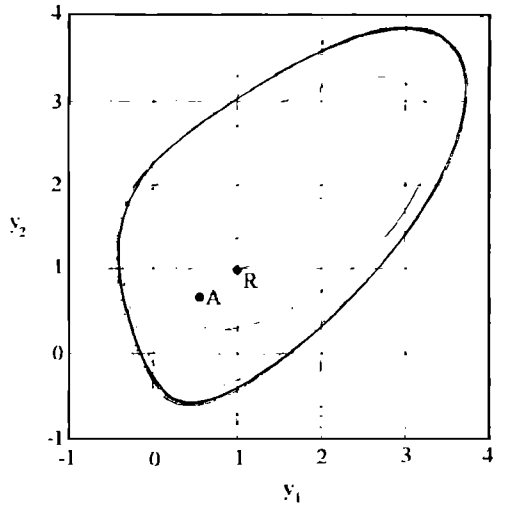

FIG. 6. Phase plane plot in the y_1-y_2 plane for the typical values of Table I (p_s=1.91 and α=0.76: point P_1 in Fig. 5). The analytical locations of equilibrium positions R and A are indicated.

Finally, the plot in Fig. 9 was obtained using the values α=0.9 and p_s=1 (point P_4 in Fig. 5), which corresponds to the region where equilibrium position R is stable and equilibrium position A is unstable. An initial position y_{1e}=0.12 and y_{2e}=0.21 was used, which is the analytical location of equilibrium position A. As before, the real location of equilibrium position R can be obtained as the center of the trajectory with the result y_{1e}=1.13 and y_{2e}=1.10, which is close to the analytical result $y_{1e}=y_{2e}=1$.

IV. CONVERGENT AND DIVERGENT PREPHONATORY GLOTTIS

A. Convergent prephonatory glottis

The case of a convergent prephonatory glottis, i.e., $x_{10}>x_{20}$, is briefly considered here. The analysis is restricted to the particular case given by a coupling ratio α=0.76, k_1/k_2=10 (same as in Fig. 4), and β=1.1. The locations of the equilibrium positions in the y_1-y_2 plane with p_s as a parameter are shown in Fig. 10, obtained solving the system of equations (8) and (13) with the above values.

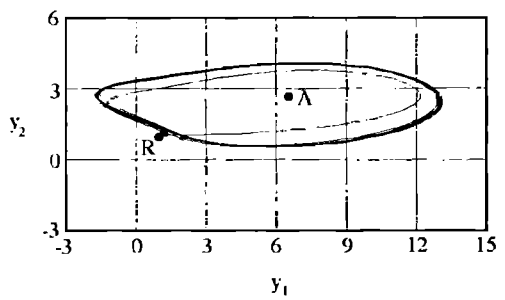

FIG. 7. Phase plane plot in the y_1-y_2 plane for p_s=7.5, α=0.3, and other parameters as given in Table I (point P_2 in Fig. 5). The analytical locations of equilibrium positions R and A are indicated.

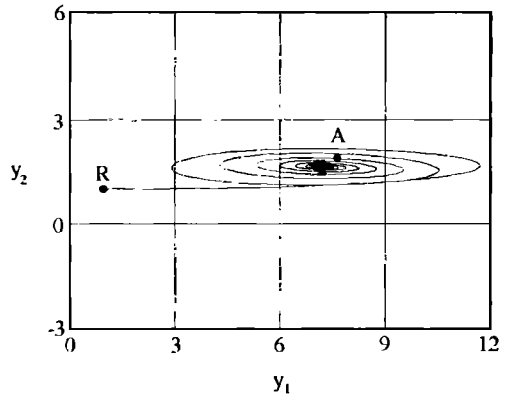

FIG. 8. Phase plane plot in the y_1-y_2 plane for p_s=7.5, α=0.15, and other parameters as given in Table I (point P_3 in Fig. 5). The analytical locations of equilibrium positions R and A are indicated.

If we compare the Fig. 10 case with the case of a rectangular glottis (Fig. 4), some similarities and differences can be noted. First, the number of equilibrium positions is the same—three; these are denoted as I, II, and III. At p_s=0.40, equilibrium positions II and III cancel each other. Equilibrium position III is equivalent to equilibrium position B in Fig. 4, since they have similar location and stability properties. In Fig. 10, however, there is no transcritical bifurcation between I and II (they never coincide). Applying a stability analysis, we find that equilibrium position II is always unstable. This implies that the oscillation region is determined only by the instability of equilibrium position I: If it is stable, the oscillation will spiral around equilibrium position I with decreasing amplitude; and if it is unstable, a limit cycle will be generated.

Equilibrium position I can be considered as equivalent to the previous equilibrium position R (at the rest position) for p_s smaller than its value at the coincidence of equilibrium positions A and R (i.e., below curve OL in Fig. 5), and equivalent to position A for p_s higher than that value (above curve OL in Fig. 5). Inversely, equilibrium

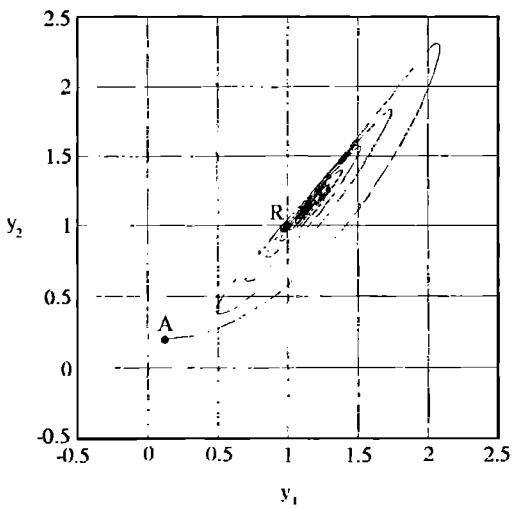

FIG. 9. Phase plane plot in the y_1-y_2 plane for p_s=1, α=0.9, and other parameters as given in Table I (point P_4 in Fig. 5). The analytical locations of equilibrium positions R and A are indicated.

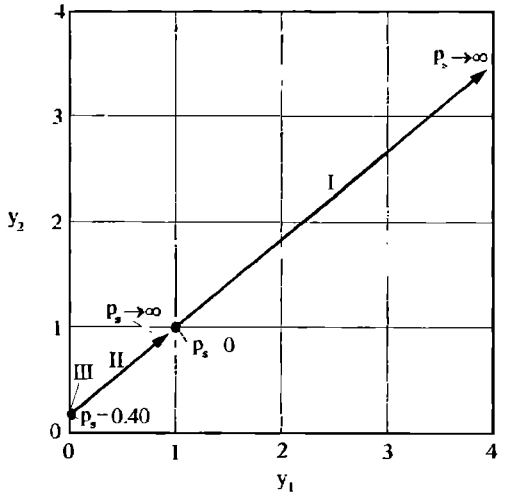

FIG. 10. Location of the equilibrium positions I, II, and III in the y_1-y_2 plane with the normalized subglottal pressure p_s as a parameter, for $k_1/k_2=10$, $\alpha=0.76$, and $\beta=1.1$ (convergent prephonatory glottis).

position II is equivalent to the previous equilibrium positions A and R, respectively (in simple words, equilibrium position I is always the equilibrium position with the biggest values of the coordinates y_{ie}, and equilibrium position II is the one with the smallest). Then, with this definition, in the case of the rectangular glottis the oscillation region is also determined by the instability of equilibrium position I.

The value of p_s at which equilibrium position I becomes unstable is $p_s=0.43$, which is higher than the value for the rectangular glottis $p_s=0.41$. Although the difference is small, it implies that a convergent glottis restricts the oscillation region, increasing the threshold pressure.

B. Divergent prephonatory glottis

The case of a divergent prephonatory glottis, i.e., $x_{10}<x_{20}$, is shown in Fig. 11. A value of $\beta=0.9$ and other parameters as in Fig. 10 were used in the calculations.

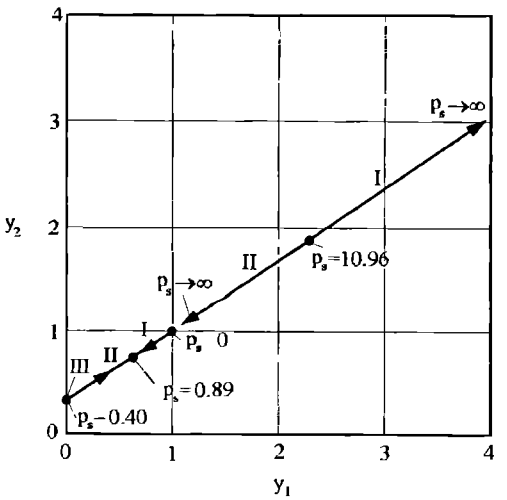

FIG. 11. Location of the equilibrium positions I, II, and III in the y_1-y_2 plane with the normalized subglottal pressure p_s as a parameter, for $k_1/k_2=10$, $\alpha=0.76$, and $\beta=0.9$ (divergent prephonatory glottis).

The number of equilibrium positions is the same as before, and they are denoted equivalently as in the case of the divergent glottis. Equilibrium positions II and III also cancel each other at $p_s=0.40$. However, note that the transcritical bifurcation of the rectangular glottis in Fig. 4 subdivides into two saddle-node bifurcations, where equilibrium positions I and II first cancel each other and then reappear. The values of p_s for those bifurcations are $p_s=0.89$ and 10.96. For values between those limits, we have the curious result that there is no equilibrium position in the system (but the limit cycle is still present). The value of p_s at which equilibrium position I becomes unstable is $p_s=0.39$, lower than the values for the rectangular and convergent glottis; i.e., the divergent glottis helps the oscillation decreasing the threshold pressure.

V. DISCUSSION OF THE RESULTS

First, it is important to point out that the existence of more than one equilibrium position does not seem to be just a mathematical characteristic of the model without a physiological correlate. As explained by Titze (1988), the aerodynamic forces act pushing the vocal folds appart in a convergent glottis, and sucking them together in a divergent one. Thus, it seems natural to have at least two equilibrium positions, one in a convergent and wide glottis and the other in a divergent and narrow glottis, where the aerodynamic forces balance the elastic restoring forces of the vocal folds. Note in Fig. 10 that at equilibrium position I the glottis is convergent and wider than at the rest position, i.e., $y_{1e}>y_{2e}$ and $y_{1e}>1$, $y_{2e}>1$; whereas at equilibrium position II it is divergent and narrower, i.e., $y_{1e}<y_{2e}$ and $y_{1e}<1$, $y_{2e}<1$.

In his work, Titze (1988) also showed the existence of a secondary equilibrium position, which is the position assumed by the vocal folds when the air is flowing. That secondary position is equivalent to the present equilibrium position I: Both are located at the rest position for a subglottal pressure equal to zero and move to widen or narrow the glottal area in a convergent or divergent prephonatory glottis, respectively, when the subglottal pressure is increased from zero. Since small-amplitude oscillations around this secondary possition were assumed by Titze, his analysis did not show the other equilibrium positions (II and III) and related bifurcations. For that reason, some differences with his results can be noted; e.g., in the case of the rectangular glottis, the secondary position is located at the rest position, whereas equilibrium position I is at the rest position only for a subglottal pressure lower than the value corresponding to the transcritical bifurcation. Also, Titze's equations show that the secondary equilibrium position dissapears at a certain subglottal pressure in a divergent prephonatory glottis, but do not show that it reappears at a higher value of the subglottal pressure, as in Fig. 11.

In spite of the differences, the results support Titze's approach to analyze the vocal fold oscillation. As stated previously, the generation of the oscillation is only determined by the instability of equilibrium position I. Hence, the oscillation conditions can be studied assuming small

amplitudes around it (but not around the rest position), as in Titze's analysis. An interesting subject for further study would be the extension of his analysis to incorporate the findings of this work, such as those discussed above for the rectangular and divergent prephonatory glottis.

Considering now equilibrium position III, and noting its small region of existence, we can conclude that it probably has no significant role in the oscillation.

The results of this analysis can also be examined relative to the negative differential resistance (NDR) oscillation theory presented by Conrad and McQueen (1988). In their work, they first analyzed the semitransglottal pressure in the two-mass model, defined as the pressure drop between the subglottal value and the pressure at the junction between both masses, as a function of the air volume velocity in a steady flow condition. They then showed the existence of a region of negative differential resistance in the case of a weak coupling between the masses ($k_c/k_2 \ll 1$); i.e., a region where an increase in the air volume velocity produces a decrease of the semitransglottal pressure. Based on this result, they explained the oscillation postulating that it is generated when this negative resistance overcomes the positive resistive part of the related aerodynamic impedances. Thus, the two-mass model was linked with the previous collapsible tube model (Conrad, 1983), also based on the existence of a negative differential resistance.

However, we can see in Fig. 5 that the region of weak coupling ($\alpha \cong 0$) is outside the oscillation region. (In Conrad and McQueen's analysis, a convergent prephonatory glottis with $\beta = 1.11$ was adopted. Although Fig. 5 corresponds to $\beta = 1$, the difference is small and does not introduce a significant change in the oscillation region.) Conrad and McQueen's results show that the negative resistance appears for values of k_c/k_2 lower than approximately 8, which corresponds to a coupling ratio $\alpha = 0.11$; but we found that the minimum value of the coupling ratio for the oscillation region is $\alpha = 0.18$, which implies that the region of negative resistance is outside the oscillation region. We can then conclude that the oscillation is not caused by the existence of the negative resistance, which disproves Conrad and McQueen's theory and also questions the validity of the collapsible tube as a suitable model for the vocal folds.

VI. CONCLUSION

It has been shown that the dynamics of the vocal fold oscillation is far more complex than assumed in previous works, with the existence of more than one equilibrium position and several bifurcation phenomena. The results support the previous approach by Titze (1988) suggesting a large-amplitude extension of his work. On the other hand, they disprove the previous theory based on the existence of a negative differential resistance. These findings are important to understand the vocal fold oscillation and to set the direction for further analytical studies.

However, an important point has been left in this analysis: What do the equilibria and bifurcations mean in terms of phonation? The answer is not clear, perhaps because of the adoption of the two-mass model, as anticipated in the introductory section. We recall that the intention of this study has been to provide a first insight into the oscillation dynamics from a general large amplitude approach. Further studies with a more suitable model, such as a possible extension of Titze's model whose body-cover structure is closer to the vocal fold anatomy, will be required as a next step for a better correlation with the voice physiology. Also, experimental research will be needed to confirm and complement the analytical results.

ACKNOWLEDGMENT

I am grateful to Dr. Toshiyuki Gotoh for his support and his interest in this study.

Baer, T. (1981). "Observations of vocal fold vibration: Measurements of excised larynges," in *Vocal Fold Physiology*, edited by K. N. Stevens and M. Hirano (University of Tokyo, Tokyo), pp. 119–133.

Conrad, W. A. (1983). "Collapsible tube model of the larynx," in *Vocal Fold Physiology: Biomechanics, Acoustics, and Phonatory Control*, edited by I. R. Titze and R. C. Scherer (The Denver Center for the Performing Arts, Denver), pp. 328–348.

Conrad, W. A., and McQueen, D. M. (1988). "Two-mass model of the vocal folds: Negative differential resistance oscillation," J. Acoust. Soc. Am. **83**, 2453–2458.

Flanagan, J. L. (1972). *Speech Analysis, Synthesis and Perception* (Springer-Verlag, New York), pp. 43–50.

Guckenheimer, J., and Holmes, P. (1983). *Nonlinear Oscillations, Dynamical Systems, and Bifurcations of Vector Fields* (Springer-Verlag, New York), pp. 12–16 and 145–156.

Ishizaka, K. (1981). "Equivalent lumped-mass models of vocal fold vibration," in *Vocal Fold Physiology*, edited by K. N. Stevens and M. Hirano (University of Tokyo, Tokyo), pp. 231–244.

Ishizaka, K., and Flanagan, J. L. (1972). "Synthesis of voiced sounds from a two-mass model of the vocal cords," Bell Syst. Tech. J. **51**, 1233–1268.

Ishizaka, K., and Flanagan, J. L. (1977). "Acoustic properties of longitudinal displacement in vocal cord vibration," Bell Syst. Tech. J. **56**, 889–918.

Ishizaka, K., and Isshiki, N. (1976). "Computer simulation of pathological vocal-cord vibration," J. Acoust. Soc. Am. **60**, 1193–1198.

Ishizaka, K., Kaneko, T., and Matsumura, M. (1987). "Natural frequencies of the vocal folds and voice pitch," Rep. Tech. Comm. Speech Acoust. Soc. Jpn. **SP86-119**, 31–37 (in Japanese).

Ishizaka, K., and Matsudaira, M. (1972). "Theory of vocal cord vibration," Rep. Univ. Electro-Comm. Sci. Tech. Sect. **23**, 107–136.

Koizumi, T., Taniguchi, S., and Hiromitsu, S. (1987). "Two-mass models of the vocal cords for natural sounding voice synthesis," J. Acoust. Soc. Am. **82**, 1179–1192.

Lucero, J. C. (1993). "The dynamics of the vocal fold oscillation," Ph.D. dissertation, Graduate School of Electrical Science and Technology, Shizuoka University, Japan.

Lucero, J. C., and Gotoh, T. (1992). "Equilibrium positions in the plank model of the vocal cords and stability analysis," Proceedings of the 1992 Autumn Meeting of the Acoustical Society of Japan, pp. 343–344.

Miller, J. A., Pereira, J. C., and Thomas, D. W. (1988). "Fluid flow through the larynx channel," J. Sound Vib. **121**, 277–290.

Titze, I. (1988). "The physics of small-amplitude oscillation of the vocal folds," J. Acoust. Soc. Am. **83**, 1536–1552.